The Henryk Niewodniczański
INSTITUTE OF NUCLEAR PHYSICS
Polish Academy of Sciences
ul. Radzikowskiego 152, 31-342 Kraków, Poland

www.ifj.edu.pl/publ/reports/2016/

Kraków, March 2016

Report No 2090/AP

Calculations of neutron and gamma energy spectra in surroundings of the HRNS for ITER

Grzegorz Tracz

Abstract

An optimisation of the High Resolution Neutron Spectrometer HRNS) shield was performed. Concrete and polyethylene shields of different thicknesses were considered. Two boxes for two sets of detectors are to be built of polyethylene though the underside is planned to be made of concrete. The final external dimensions of the first box are to be 175 cm (length), 150 cm (width) and 170 cm (height) while the second box is to be 215 cm long, 150 cm wide and 200cm high. All the shield elements are to be 10 cm thick including a wall between the boxes.

Next, photons and scattered neutrons spectra in the first box detectors were calculated. The results will be used as a source to estimate the background contribution on the different detectors.

Finally, the neutron and photon spectra through the inner and outer surfaces of the first box were computed. The results are to be used as gamma and neutron sources in subsequent evaluations of shut-down dose rates in the port cell.

A detailed MCNP input file was elaborated, based on a CAD model, which geometric part contains over 600 cells of HRNS, not counting void.

1 Introduction

ITER is to be the world's largest experimental nuclear fusion reactor. Like other tokamaks, it requires numerous diagnostics systems to control the synthesis of hydrogen isotopes.

The High Resolution Neutron Spectrometer (HRNS) is a set of detectors designed for ITER. First of all, HRNS is to provide information concerning the ratio of tritium and deuterium ion densities in plasma. Moreover, it is to measure the fuel ion temperature and energy distributions as well as neutron spectra. The expected neutron flux at the HRNS inlet is $\sim 10^9$ $n \cdot s^{-1} \cdot cm^{-2}$ for a 5 cm radius aperture in the first ITER wall.

The detectors are arranged in two groups. So called 'low efficiency' spectrometers closer and 'high efficiency' counters farther from the tokamak. A collimator between the groups is considered to enhance the system.

The first set of detectors forms the thin-foil proton recoil (TPR) system. Neutrons are converted to charged particles in the foils and recoil proton energy is registered in a silicon solid state detector.

The time-of-flight technique is employed by the high efficiency system (TOFOR) for detection of 2.45 MeV and 14 MeV neutrons from the plasma. A particle is scattered in two (sets of) detectors. The first one starts while the second one stops the measurement of the time interval between the scatterings in order to evaluate the neutron energy.

2 HRNS shield optimisation

A number of Monte Carlo calculations were carried out to optimise the HRNS shield. The computer simulations were performed with the MCNP5 code [1]. All the results (fluxes and doses) presented in the foregoing study are computed per one source neutron. Consequently, all fluxes are in cm^{-2} while doses in Sv. The regular units ($cm^{-2} \cdot s^{-1}$, $Sv \cdot s^{-1}$) can be obtained by multiplying obtained results by the total number of neutrons emitted per second from ITER.

At first solely the first box was examined then the other cuboid was added. Their outer dimensions changed and were imposed by engineering constraints and were nor the subject of investigations or optimisations in this study.

In this chapter it is assumed the source emits 2.45 MeV and 14 MeV neutrons with the equal probability.

2.1 Configuration I

The geometry modelled in the initial simulations is presented in Figure 1. As mentioned, merely the first box was investigated. The thickness of the shield varies from 5 cm up to 25 cm with the step of 5 cm. Concrete and polyethylene were examined as the possible shield materials. The steel cylinder to contain detectors is situated so that it touches the opening of the shield for all its thickness.

Total fluxes (i.e. integrated over energy) of neutrons and photons inside the entire cylinder volume were calculated, but only particles scattered and/or created in the shield were tallied. Moreover, neutron and photon doses in a sphere of 9 cm radius centred 10 cm behind the lateral surface of the shield were computed. The sphere is presented in the horizontal cross-section of Configuration I (Figure 2).

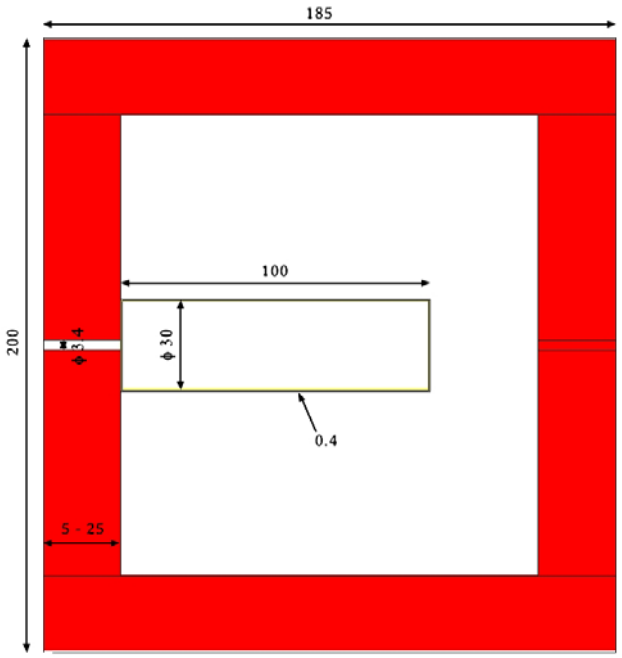

Figure 1 Vertical cut of Configuration I modelled in the first step of simulations (dimensions in cm)

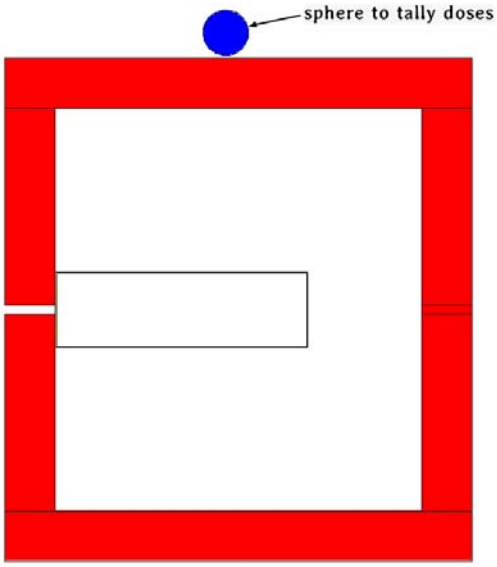

Figure 2 Horizontal cut of Configuration I modelled in the first step of simulations.

Results of the simulations for neutrons (Figure 3) show that the dose decreases roughly 3.5 times when the shield gets thicker from 5 cm to 25 cm. Polyethylene provides better shielding, contrary to photons (Figure 4). The thicker the shield, the more photons are created and the dose is much lower for concrete. Figure 5 presents the total dose of neutrons and photons for the examined materials. Polyethylene ensures much better shielding, even more than two times, since the neutron dose is significantly higher than the photon one.

Both neutron and photon fluxes inside the cylinder increase roughly linearly and do not differ significantly for polyethylene and concrete. The neutron flux grows even more than 7 times, while the photon flux less than three times.

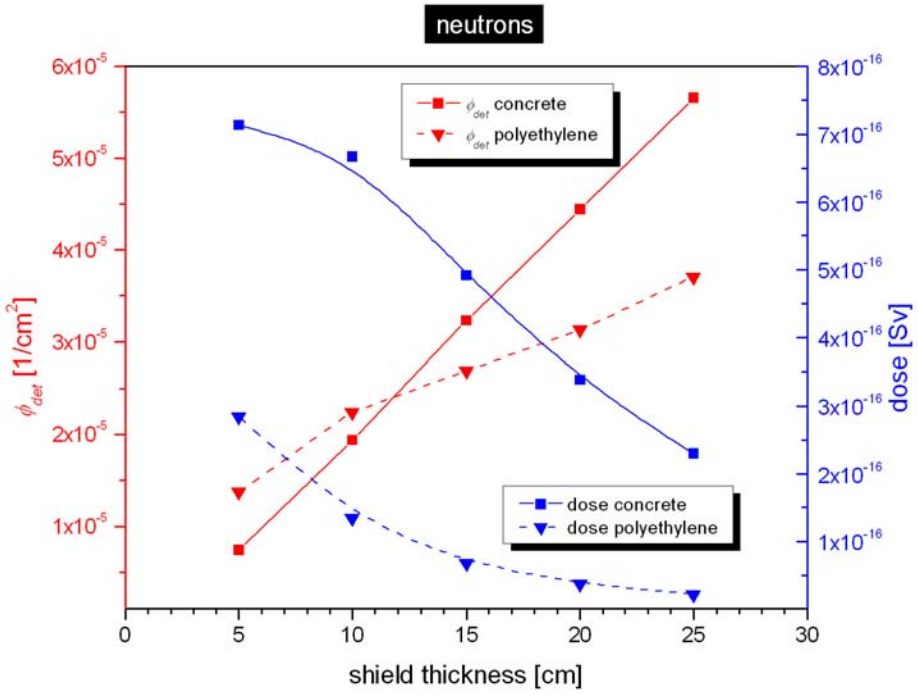

Figure 3 Neutron fluxes in the cylinder and doses outside the shield in Configuration I.

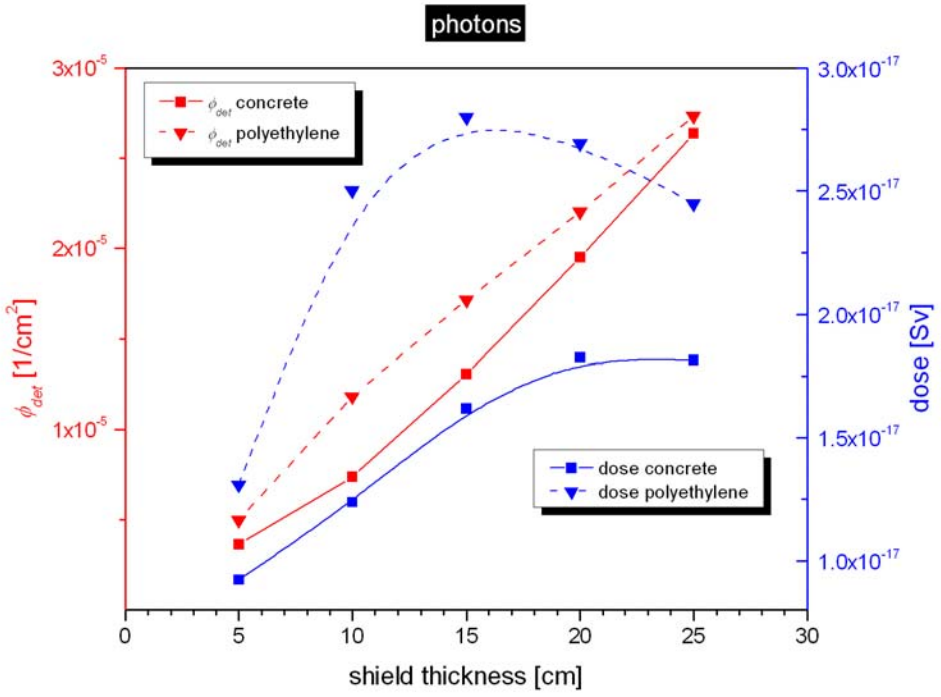

Figure 4 Photon fluxes in the cylinder and doses outside the shield in Configuration I.

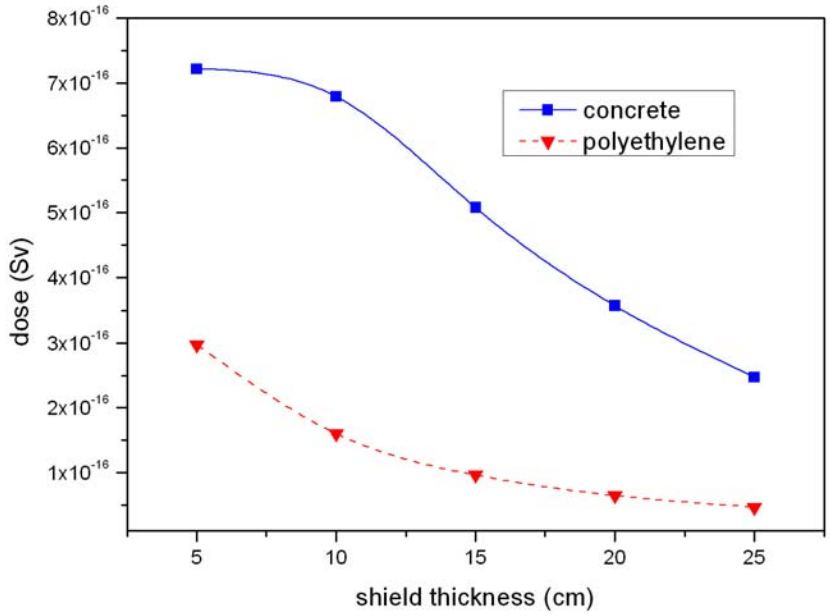

Figure 5 Total dose of neutrons and photons for concrete and polyethylene in Configuration I.

2.2 Configuration II

In the second step of simulations the arrangement was modified so that an opening of the same diameter as the inlet was added at the exit of the shield. Besides, three polyethylene plates to scatter the beam, each of 0.17 mm thickness and of 10 cm^2 area, was placed inside the cylinder as presented in Figure 6.

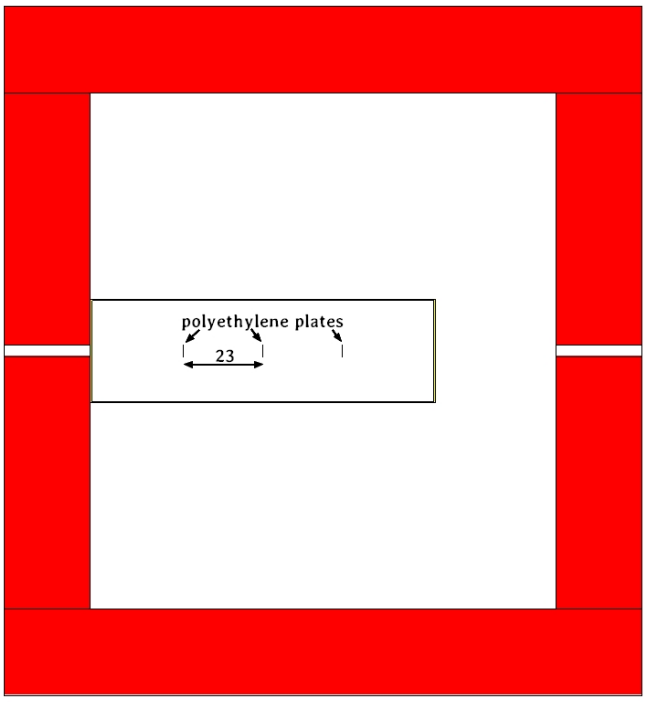

Figure 6 Vertical cut of Configuration II (dimension in cm).

The results of calculations (Figure 7, Figure 8 and Figure 9) show that the absolute values of fluxes and doses decreased while the appearance of the curves essentially remained the same.

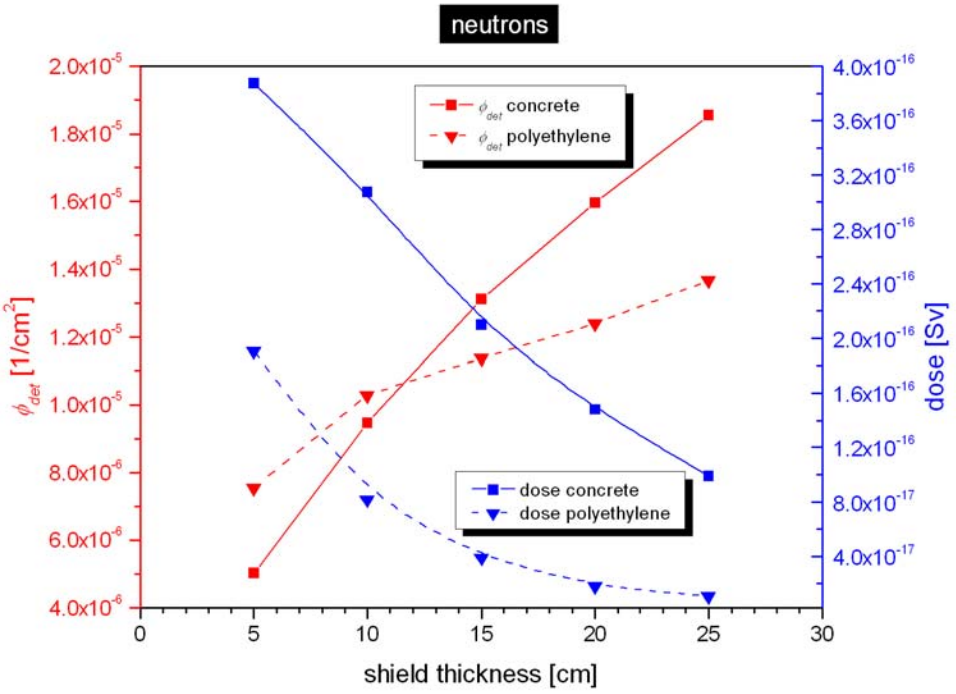

Figure 7 Neutron fluxes in the cylinder and doses outside the shield in Configuration II.

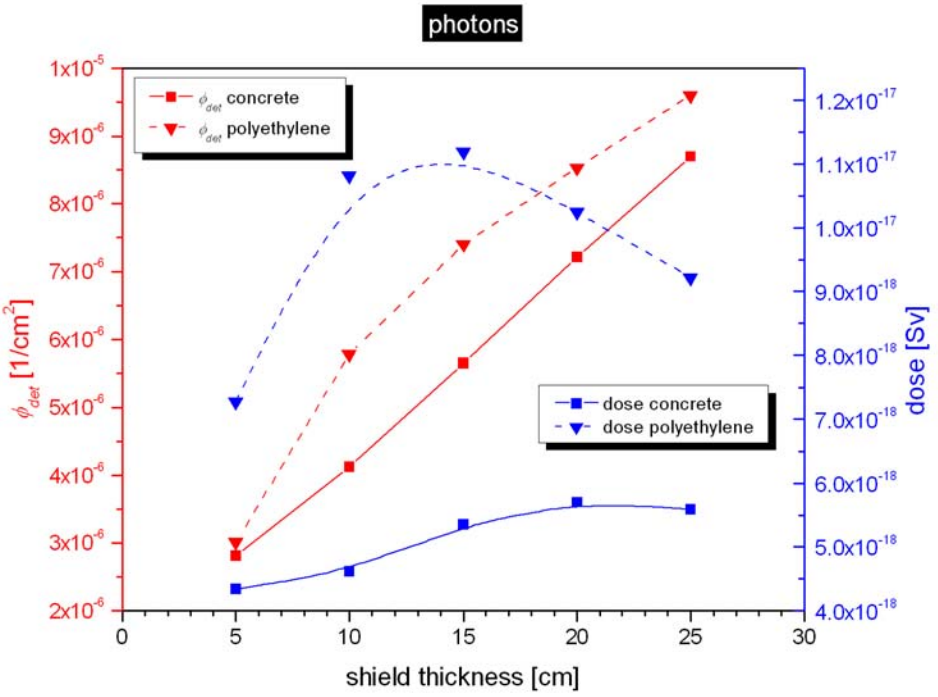

Figure 8 Photon fluxes in the cylinder and doses outside the shield in Configuration II.

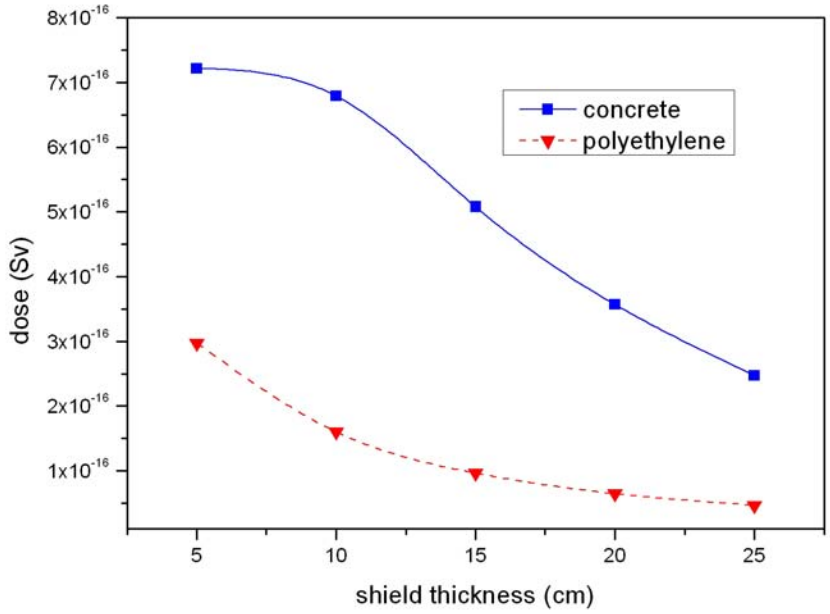

Figure 9 Total doses of neutrons and photons for concrete and polyethylene outside the shield in Configuration II.

The next set of graphs (Figure 10, Figure 11 and Figure 12) presents relative values. The fluxes and doses obtained for the second arrangement were normalized (divided) to the results obtained in Configuration I. Because the opening at the shield outlet was filled with air, the neutron beam did not scatter on concrete or polyethylene. As a result of that both the neutron and photon fluxes as well as the doses significantly diminished, even almost three times for the thickest shields. The total doses for the examined materials roughly halved.

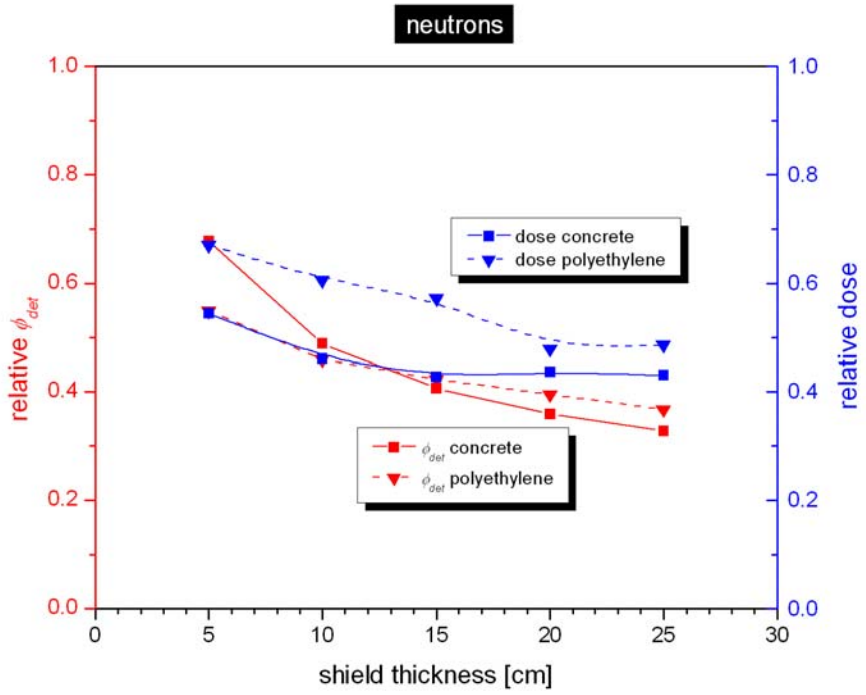

Figure 10 Relative neutron fluxes in the cylinder and doses outside the shield normalised to Configuration I.

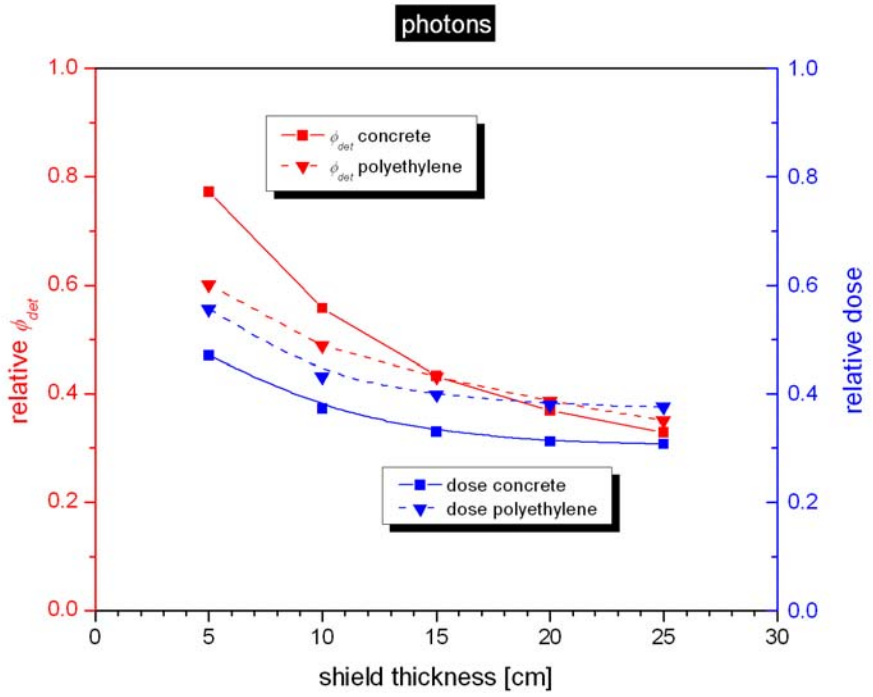

Figure 11 Relative photon fluxes in the cylinder and doses outside the shield normalised to Configuration I.

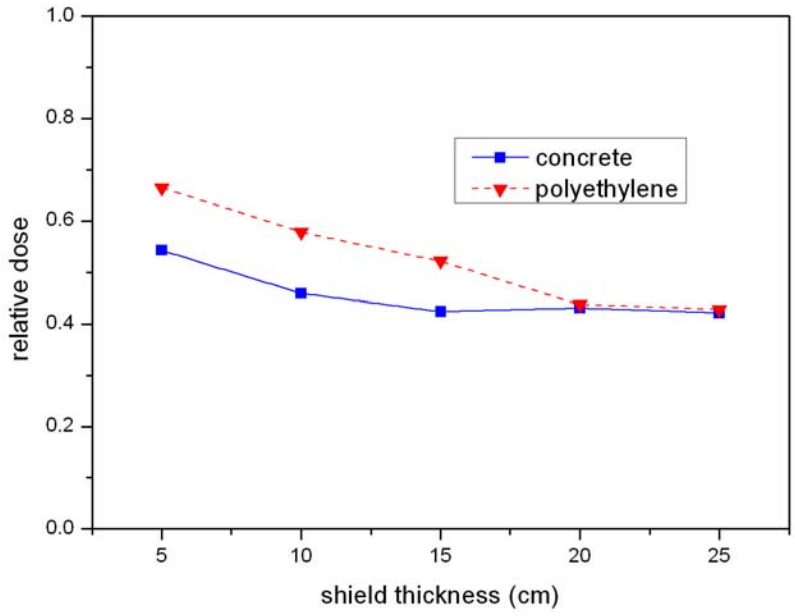

Figure 12 Relative total doses of neutrons and photons for concrete and polyethylene normalised to Configuration I.

2.3 Configuration III

In the next simulations the second box containing a set of detectors was added to the model (Figure 13). Based on the obtained Monte Carlo results the 10 cm shield was chosen for further considerations. The dimensions of the cylinder in the first box and polyethylene plates inside it were not modified whereas the tube was shifted away from the

inlet. Like previously, the concrete and polyethylene shielding were examined. Another variant without the wall between the boxes was also investigated (Figure 14).

Since the neutron beam from ITER is divergent the inlet in Configuration III is smaller (3.4 cm diameter) than the outlet and the hole in the wall between the boxes, both of 5 cm diameter. Previously, i.e. in Configuration II, both openings in the first box were of the same 3.4 cm diameter.

Although the time of flight set of detectors was modelled in the second box it was not directly employed either for Configuration III or in succeeding calculations. Owing to these elements scattering effects occurring at detectors and shielding walls of the second cuboid were included, which may affect results for the first box.

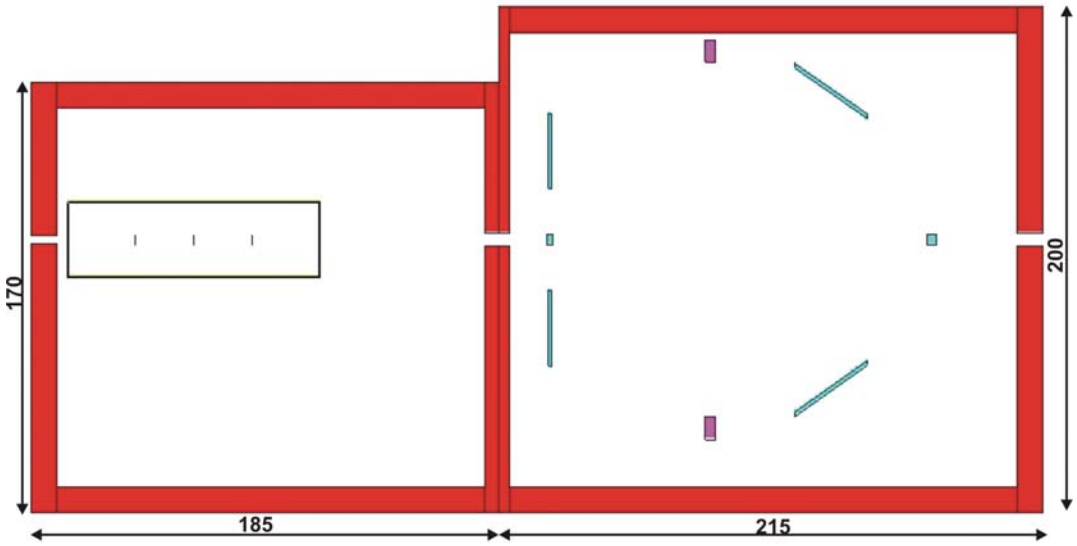

Figure 13 The vertical cut of the modelled geometry for two boxes (dimension in cm).

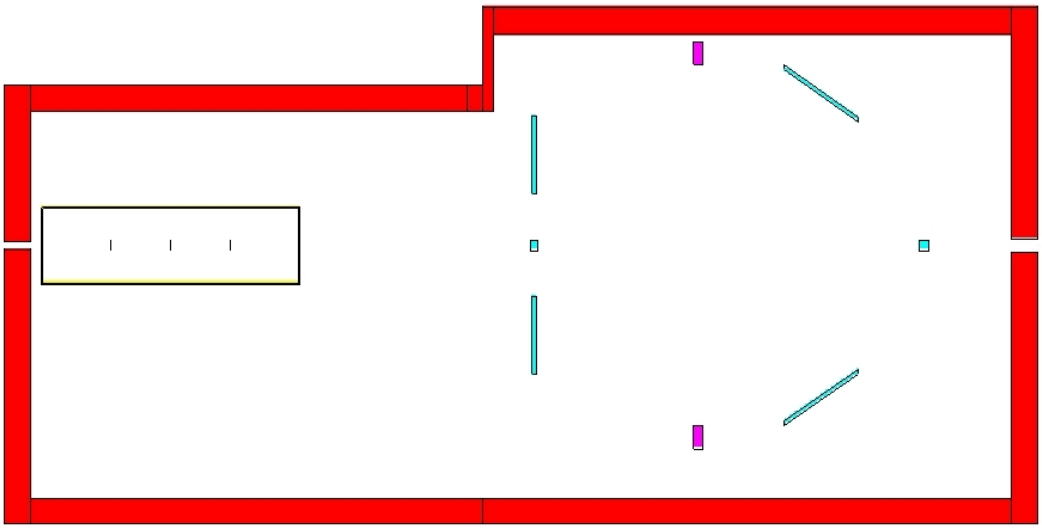

Figure 14 The vertical cut of the modelled geometry without the wall between the boxes.

Table 1 presents the fluxes inside the cylinder and the doses 10 cm behind the lateral surface of the first box shield for the both studied shielding materials and three configurations presented in Figure 6, Figure 13 and Figure 14. The doses were tallied in the same sphere as for Configuration I presented in Figure 2. No doses were calculated outside the second box.

Table 2 features the relative fluxes and doses in question. The arrangement with one cuboid (Figure 6) is considered as the reference case.

Table 1 Comparison of fluxes in the cylinder and doses outside the first box.

	neutron flux [cm^{-2}]	photon flux [cm^{-2}]	neutron dose [Sv]	photon dose [Sv]	total dose [Sv]
1 box concrete	9.47e-06	4.13e-06	3.07e-16	4.62e-18	3.12e-16
polyethylene	1.03e-05	5.78e-06	8.18e-17	1.08e-17	9.27e-17
2 boxes concrete	1.12e-05	4.16e-06	4.69e-16	8.05e-18	4.77e-16
polyethylene	1.02e-05	6.19e-06	1.22e-16	1.77e-17	1.40e-16
2 boxes merged concrete	1.10e-05	3.77e-06	4.99e-16	7.86e-18	5.07e-16
polyethylene	1.17e-05	6.45e-06	1.35e-16	1.87e-17	1.54e-16

Table 2 Relative fluxes in the cylinder and doses outside the first box.

	neutron flux	photon flux	neutron dose	photon dose	total dose
2 boxes concrete	1.18	1.01	1.53	1.74	1.53
polyethylene	0.99	1.07	1.50	1.64	1.51
2 boxes merged concrete	1.16	0.91	1.62	1.70	1.62
polyethylene	1.14	1.12	1.65	1.73	1.66

The neutron and photon fluxes essentially remained the same. The largest difference is 18 % for the neutron flux and the concrete shield in the case of the two separate cuboids.

In contrast, the total dose increased 51 % up to 66 %. The photon dose growth was even higher but the total dose is determined by neutrons. More photons are created in the additional shielding of the second box and, first of all, neutrons that previously left HRNS are scattered at the elements located in the second segment.

The configuration showed in Figure 13 provides the total doses slightly lower while the neutron flux is essentially the same for concrete and a bit higher for polyethylene.

3 Spectra of photons and scattered neutrons in the detectors placed in the first box

Monte Carlo simulations were carried out to calculate spectra of photons and scattered neutrons inside a diamond and silicon TPR detectors. The 0.3 mm thick silicon plates were of 4.6 cm inner and 10 cm outer diameters. The 1 cm thick diamond detector was

of 3 cm diameter. The results will be used as a source to estimate the background contribution on the different detectors.

The modelled arrangement is presented in Figure 15 and consists of two boxes with a simplified set of the detectors. All blue elements are scintillators made of polyvinyltoluen BC-418. Two violet rectangles are the vertical cut of an aluminium support. Both scintillators A and B are 3 cm thick and their widths and heights are 4 cm. The detectors ring is 1.6 cm thick while its inner and outer diameters are 40 cm and 100 cm, respectively. The conical ring is of the same thickness whilst its inner diameter is 96 cm and the outer 140 cm. Both detectors rings and the aluminum support are of cylindrical symmetry in regard to the beam and consequently the openings in the shield.

On the grounds of results presented in the previous chapter, it was decided the floor is to be made of concrete, while other parts of the shielding of polyethylene. The shield thickness is to be 10 cm.

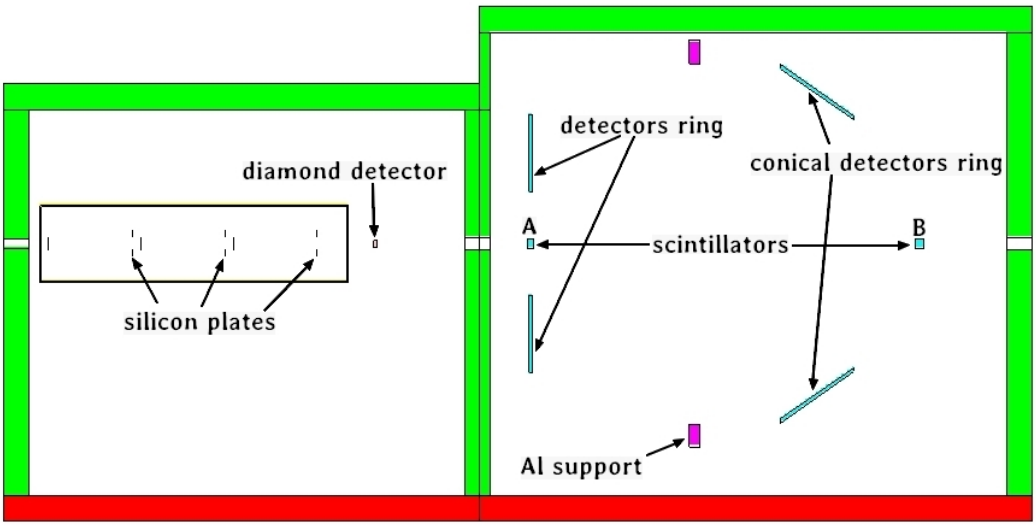

Figure 15 The vertical cross-section of the MCNP model used in the simulations. The detectors are of cylindrical symmetry.

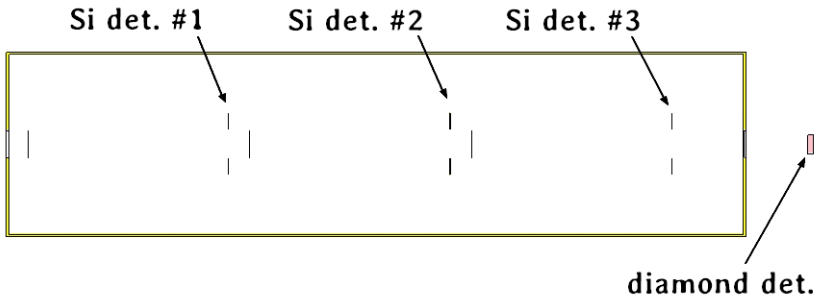

Figure 16 The arrangement of detectors in the vacuum tube and the diamond in the first box.

The set-up of the detectors in the first box is showed more detailed in Figure 16. The silicon detectors are placed in a vacuum tube, which has two windows at the inlet and outlet of the beam of 0.2 mm to minimize neutron scattering. Three polyethylene plates are to scatter the beam neutrons. The diamond detector is situated outside the cylinder in air.

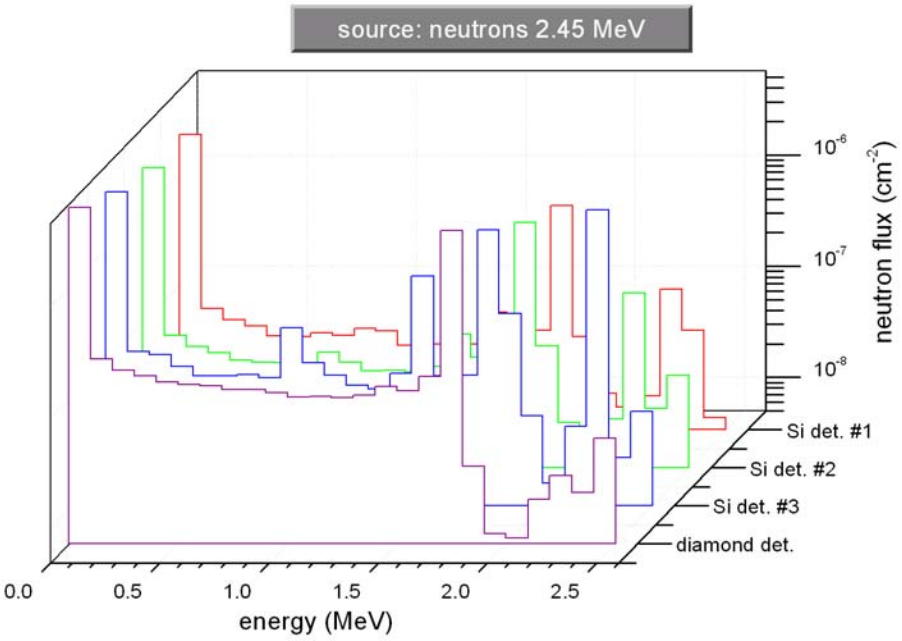

Figure 17 Scattered neutron spectra for the neutron 2.45 MeV beam in the entire volume of detectors.

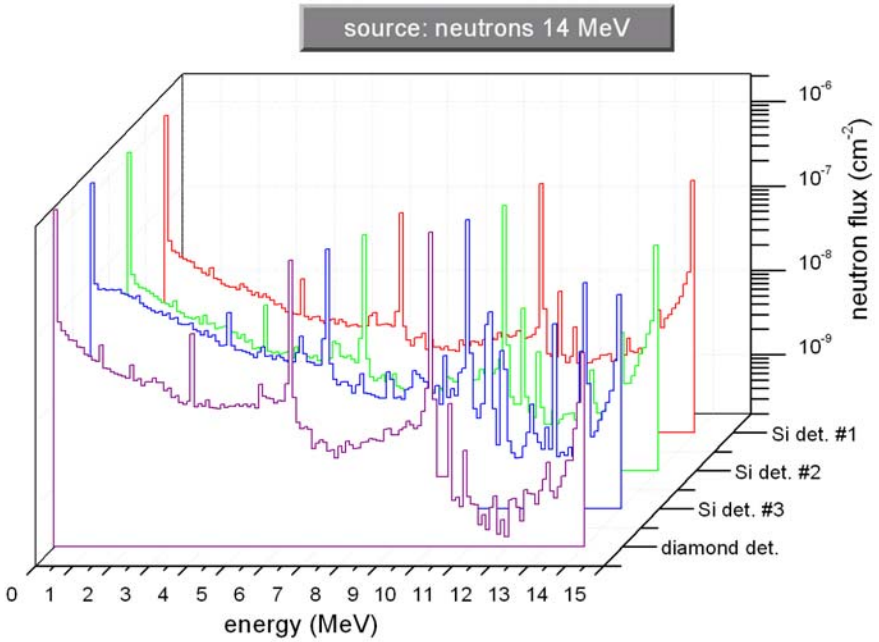

Figure 18 Scattered neutron spectra for the neutron 14 MeV beam in the entire volume of detectors.

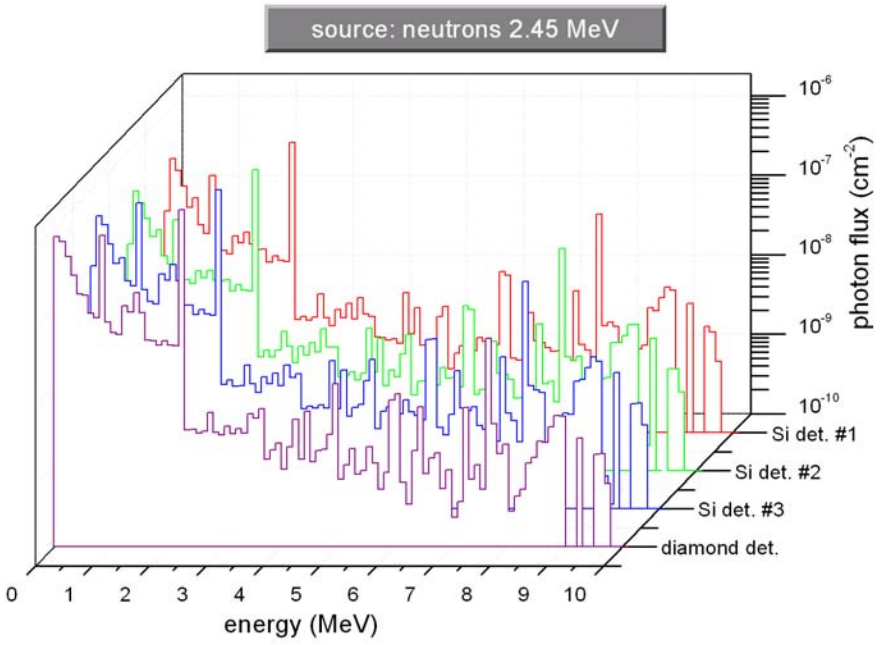

Figure 19 Photon spectra for the neutron 2.45 MeV beam in the entire volume of detectors.

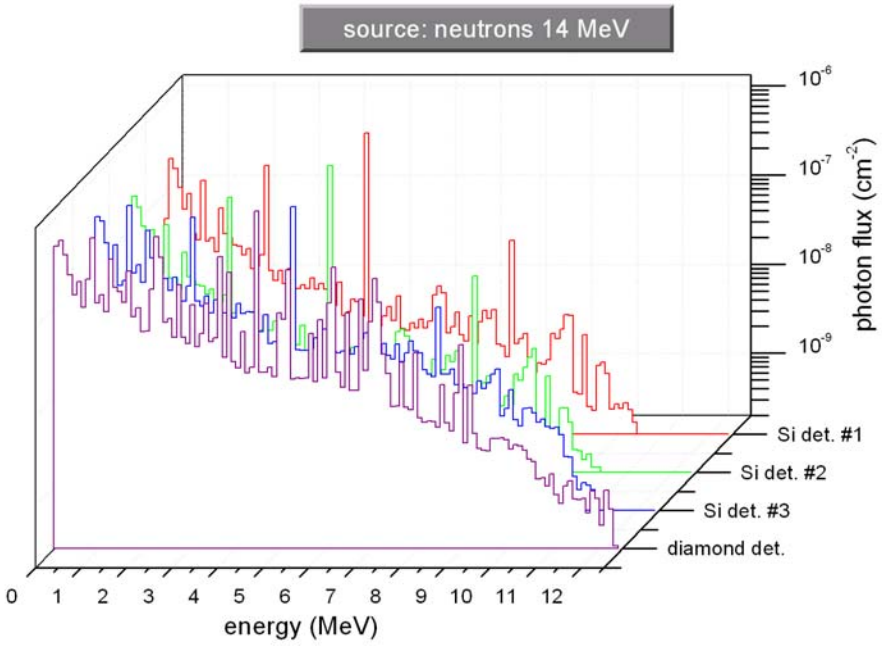

Figure 20 Photon spectra for the neutron 14 MeV beam in the entire volume of detectors.

The direct neutrons of the beam were not taken into account in the calculations of neutron fluxes. An MCNP technique called 'flagging' was used to consider solely neutrons scattered at any element of the model apart the inlet window and the polyethylene plates. In case of the diamond the neutrons that only crossed the outlet window were also excluded from tallying.

Moreover, the spectra of photons created in neutron interactions were computed.

A point source was placed 10 m in front of the first cuboid and emitted neutrons with divergence of 0.9°. The simulations were performed separately for 2.45 MeV and 14 MeV beams. Consequently, the final background contribution will be obtained as a sum of two components with appropriate weights, which will be known in future when neutron the spectrum from ITER is measured.

As expected, the beam is strongly moderated by scatterings on the light elements, hydrogen and carbon, which comprise the polyethylene shielding. Thus, the neutron spectra (Figure 17 and Figure 18) are dominated by thermal neutrons. Two other peaks (~1.8 MeV and ~2.3 MeV for the 2.45 MeV beam as well as ~6.3 MeV and ~10 MeV for the 14 MeV beam) probably come from the beam neutrons, which scattered only one or two times.

In the photon spectra (Figure 19 and Figure 20) the hydrogen (2.22 MeV) and carbon (4.43 MeV) neutron radiative capture peaks are well visible.

4 Neutron and photon spectra through the first box shields

A new MCNP input file was elaborated based on a very detailed CAD model of HRNS, which was converted with SuperMC/MCAM (Multi-physics Coupling Analysis Modelling Program) [2]. A 15 cm thick copper collimator of 40 cm outer and 3.8 cm inner diameter in the wall between the cuboids was included. The new model consisted of over 600 cells, not counting void. TPR, TOFOR, the collimator and the neutron beam were modelled aslant, as it is planned in the real HRNS construction. The beam from the ITER port is angled 0.77° horizontally and 0.9° vertically as well as the HRNS inlet and outlet. Consequently, all detectors and their elements are arranged parallel to the beam. Figure 21 shows the vertical cut of the new model.

This model was used to compute neutron and photon spectra crossing the inner and outer surfaces of the first box in both directions. The results are to be used as gamma and neutron sources in subsequent evaluations of shut-down dose rates in the port cell. Moreover, they will enable to estimate the amount of neutrons and gammas leaking out from the first box shield. As before, the simulations were conducted for the 2.45 MeV and 14 MeV neutron beams individually. The terms ‘left’ and ‘right’ refer to the HRNS lateral walls looking at the spectrometer from the ITER port side.

For the neutron spectra through the front surface the 2.45 MeV (Figure 22 and Figure 23) and 14 MeV peaks (Figure 24 and Figure 25) directly from the beam are apparent. In the case of the other surfaces the spectra are dominated by thermal neutrons. The fluxes through the inner surfaces are more or less one order of magnitude lesser than through the outer ones. The peaks ~6.3 MeV and ~10 MeV are visible for the 14 MeV beam, but not so clearly like in the previous chapter. Moreover, the ~1.8 MeV and ~2.3 MeV peaks for the 2.45 MeV beam disappeared, what might be caused by much larger number of scatterings in the shield vicinity in comparison to the TPR detectors situated in the centre of the box.

Concerning gammas, the hydrogen (2.22 MeV) peak is apparent in the photon spectra for the both beams while the carbon (4.43 MeV) peak can be noticed actually merely for the 14 MeV neutron beam (see Figure 26 to Figure 29). Contrary to neutron results, photon spectra basically do not differ for the inner and outer surfaces since gammas are produced in neutron interactions occurring mainly in the shield.

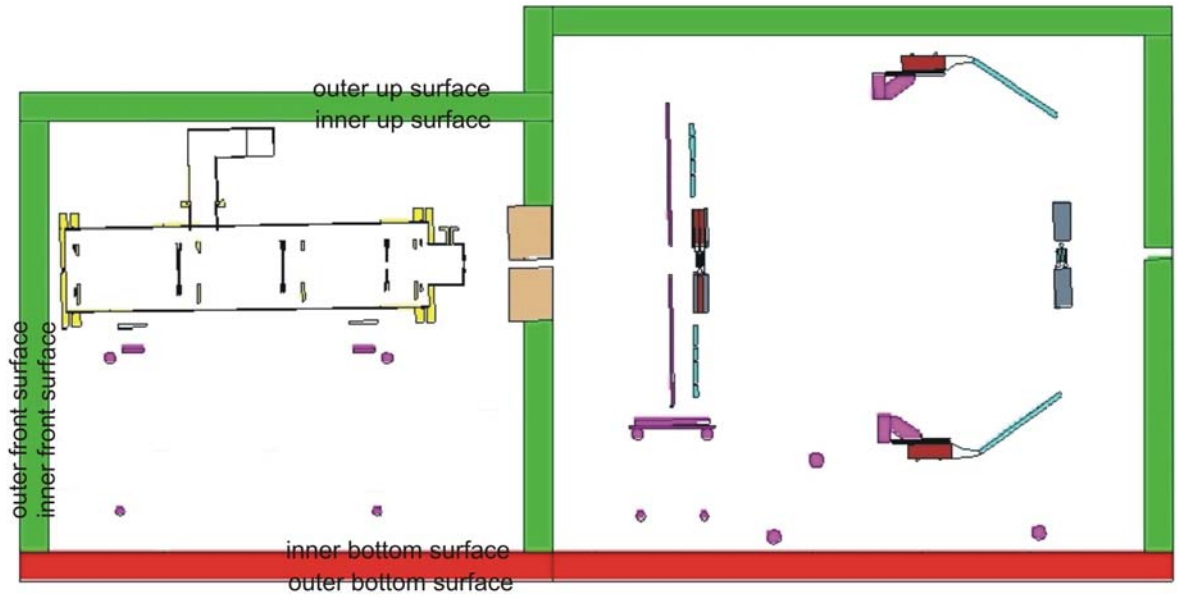

Figure 21 The vertical cross-section of the MCNP model based on a CAD file

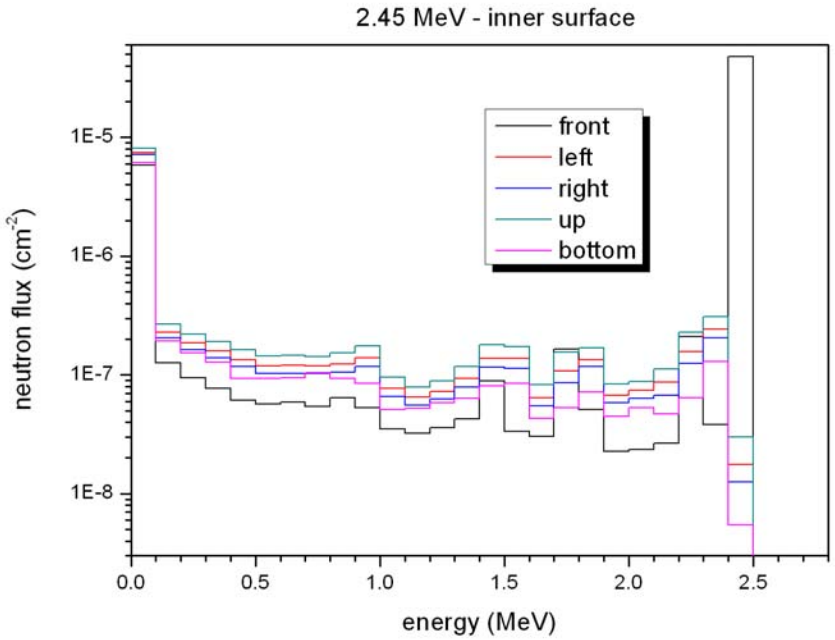

Figure 22 Neutron spectra through inner surfaces of the first box for the neutron 2.45 MeV beam

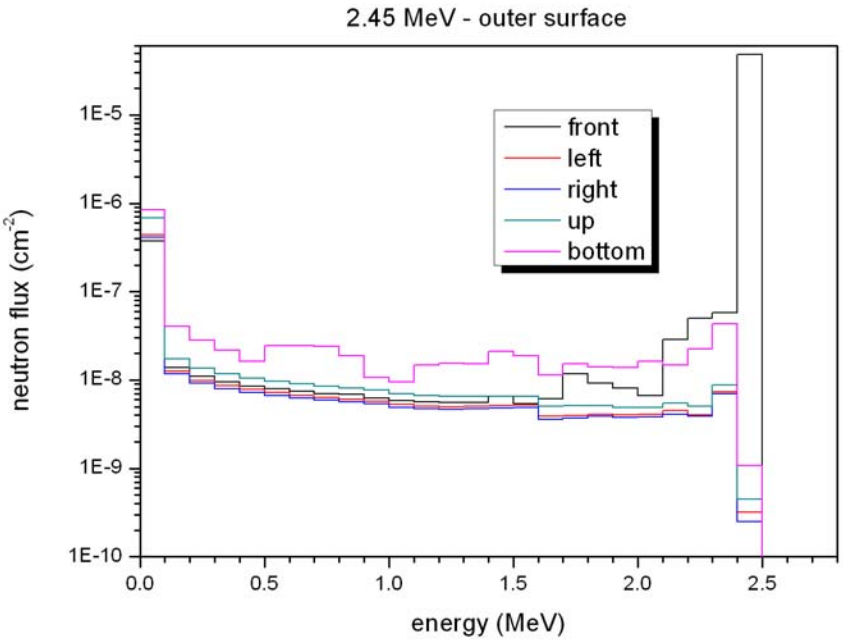

Figure 23 Neutron spectra through outer surfaces of the first box for the neutron 2.45 MeV beam

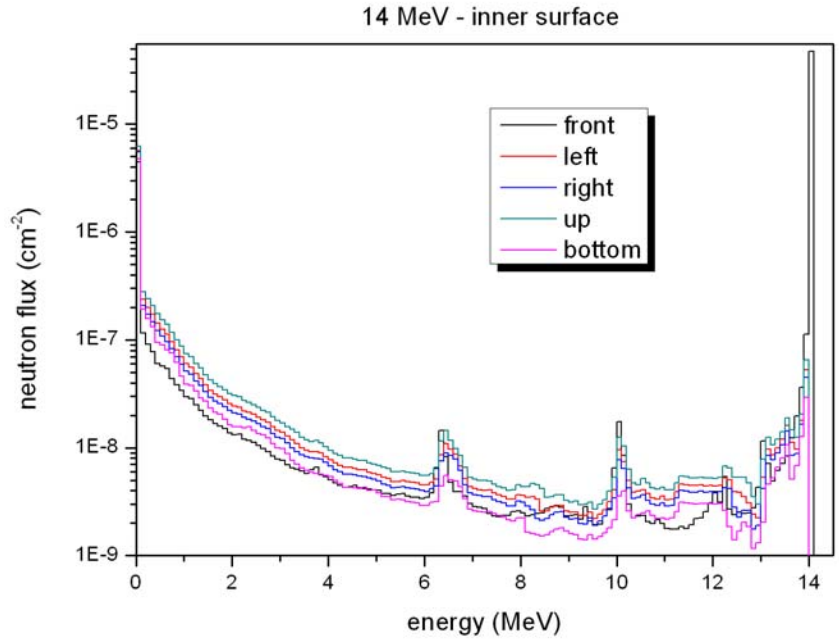

Figure 24 Neutron spectra through inner surfaces of the first box for the neutron 14 MeV beam

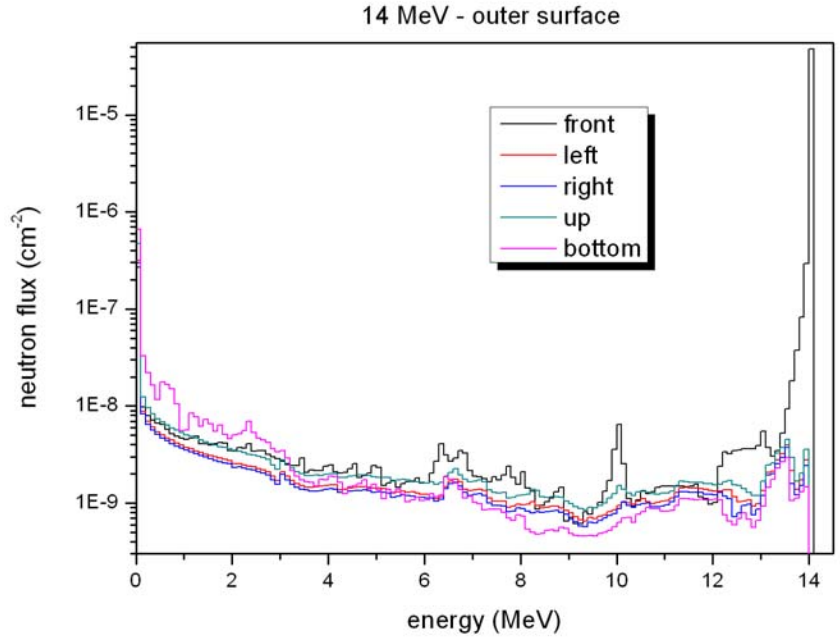

Figure 25 Neutron spectra through outer surfaces of the first box for the neutron 14 MeV beam

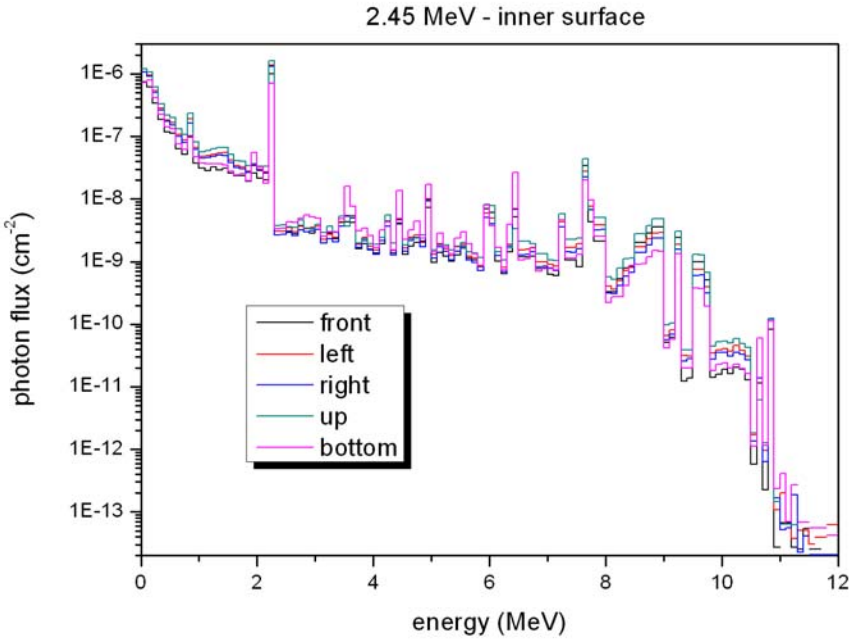

Figure 26 Photon spectra through inner surfaces of the first box for the neutron 2.45 MeV beam

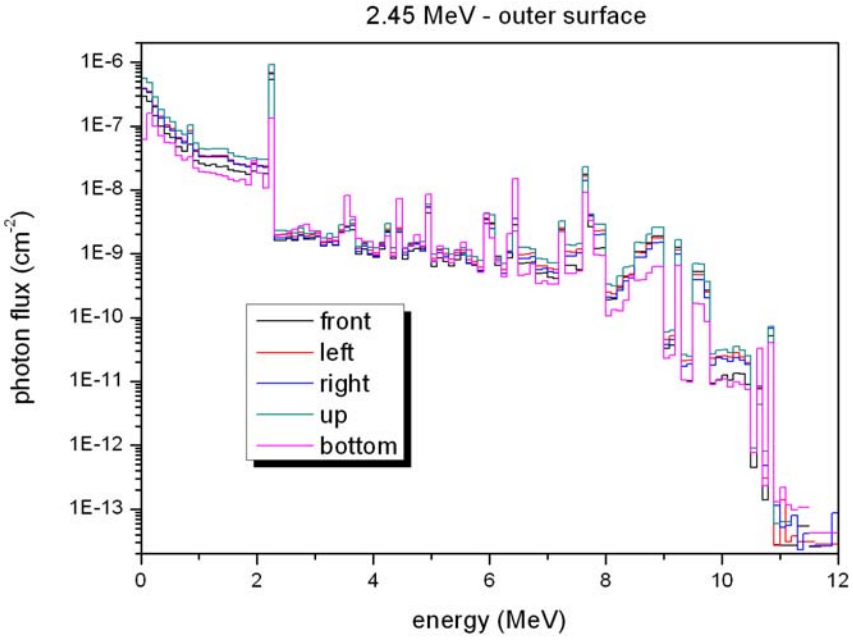

Figure 27 Photon spectra through outer surfaces of the first box for the neutron 2.45 MeV beam

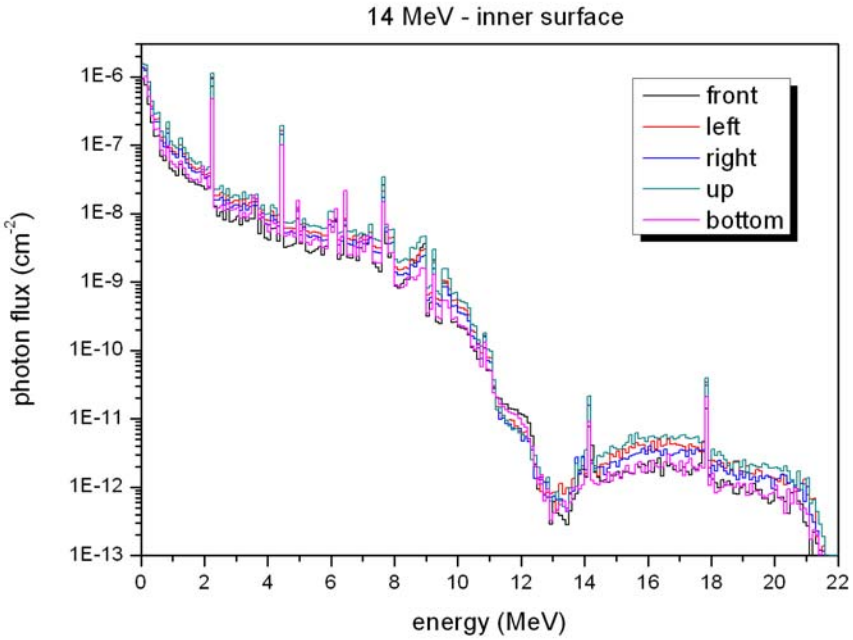

Figure 28 Photon spectra through inner surfaces of the first box for the neutron 14 MeV beam

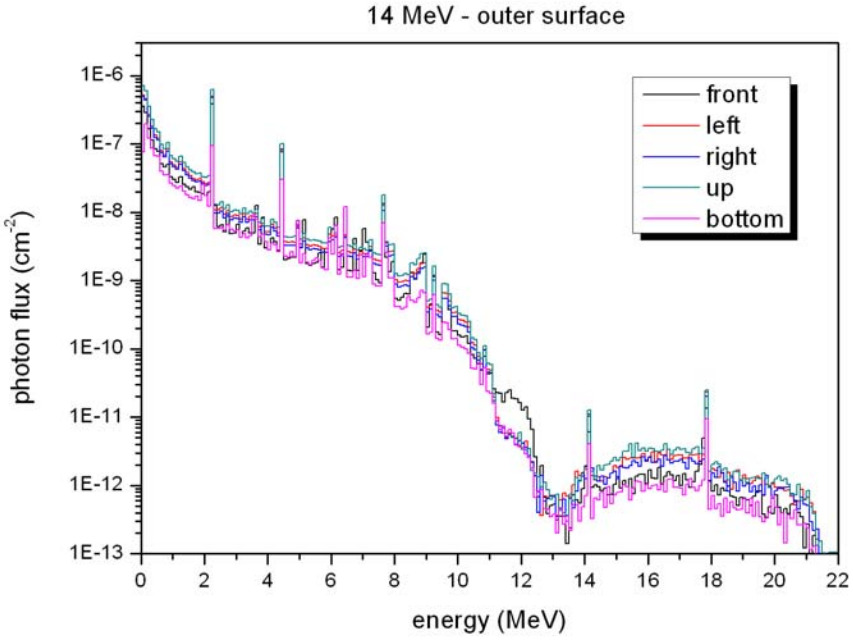

Figure 29 Photon spectra through outer surfaces of the first box for the neutron 14 MeV beam

5 Conclusions

The report features the study of three issues by means of the Monte Carlo simulations.

The first one was the optimisation of the HRNS shield. Based on the obtained results, polyethylene appears to be the best material though the underside is planned to be made of concrete. Polyethylene not only provides a better radiation shielding but also is the much lighter material than concrete. All the shield elements are to be 10 cm thick.

Afterwards, the calculations of photons and scattered neutrons spectra in the TPR detectors were presented. The results will be used as a source to estimate the background contribution on the different detectors.

Eventually, the neutron and photon spectra through the inner and outer surfaces of the first box were computed. The results are to be used as gamma and neutron sources in subsequent evaluations of shut-down dose rates in the port cell. The neutron fluxes through the outer surfaces are roughly one order of magnitude lesser than through the inner ones. The photon fluxes, in turn, remain essentially the same, because gammas are produced mostly in the shield.

The very detail MCNP input file was developed using the CAD model, which can be employed in other simulations regarding the HRNS project.

Acknowledgements

The foregoing study was implemented under the Fusion for Energy project, F4E-GRT-403, entitled “Conceptual Design and Interface Specifications of High Resolution Neutron Spectrometer” and conducted at the IFJ PAN in 2014 ÷ 2016.

The author would like to thank MSc Eng. Jerzy Kotuła for elaboration the CAD model as well as MSc Leszek Hajduk for fruitful tutorial concerning HRNS construction.

References

[1] X-5 Monte Carlo Team, *MCNP - A general Monte Carlo N-particle transport code, Version 5*, Los Alamos National Laboratory, LA-UR-03-1987, (2003)

[2] Y. Wu, FDS Team, *CAD-based interface programs for fusion neutron transport simulation*, Fusion Eng. Des. **84** (2009) 1987-1992